Star formation in *Herschel*'s Monsters versus semi-analytic models

C. Gruppioni,[1][*] F. Calura,[1] F. Pozzi,[2] I. Delvecchio,[2] S. Berta,[3] G. De Lucia,[4]
F. Fontanot,[4] A. Franceschini,[5] L. Marchetti,[6] N. Menci,[7] P. Monaco[8] and M. Vaccari[9]

[1]*Istituto Nazionale di Astrofisica - Osservatorio Astronomico di Bologna, via Ranzani 1, I-40127 Bologna, Italy*
[2]*Dipartimento di Fisica e Astronomia, Università di Bologna, viale Berti Pichat 6, I-40127 Bologna, Italy*
[3]*Max-Planck-Institut für Extraterrestrische Physik (MPE), Postfach 1312, D-85741 Garching, Germany*
[4]*Istituto Nazionale di Astrofisica - Osservatorio Astronomico di Trieste, Via Tiepolo 11, I-34143 Trieste, Italy*
[5]*Dipartimento di Astronomia, Università di Padova, vicolo dell'Osservatorio 3, I-35122 Padova, Italy*
[6]*Department of Physical Sciences, The Open University, Milton Keynes MK7 6AA, UK*
[7]*INAF Osservatorio Astronomico di Roma, via di Frascati 33, I-00040 Monte Porzio Catone, Italy*
[8]*Dipartimento di Fisica, Sezione di Astronomia, via Tiepolo 11, I-34143 Trieste, Italy*
[9]*Astrophysics Group, Department of Physics, University of Western Cape, Bellville 7535, Cape Town, South Africa*

ABSTRACT

We present a direct comparison between the observed star formation rate functions (SFRFs) and the state-of-the-art predictions of semi-analytic models (SAMs) of galaxy formation and evolution. We use the PACS Evolutionary Probe Survey and *Herschel* Multi-tiered Extragalactic Survey data sets in the COSMOS and GOODS-South fields, combined with broad-band photometry from UV to sub-mm, to obtain total (IR+UV) instantaneous star formation rates (SFRs) for individual *Herschel* galaxies up to $z \sim 4$, subtracted of possible active galactic nucleus (AGN) contamination. The comparison with model predictions shows that SAMs broadly reproduce the observed SFRFs up to $z \sim 2$, when the observational errors on the SFR are taken into account. However, all the models seem to underpredict the bright end of the SFRF at $z \gtrsim 2$. The cause of this underprediction could lie in an improper modelling of several model ingredients, like too strong (AGN or stellar) feedback in the brighter objects or too low fallback of gas, caused by weak feedback and outflows at earlier epochs.

Key words: galaxies: evolution – galaxies: formation – galaxies: star formation – cosmology: observations – infrared: galaxies.

1 INTRODUCTION

The study of how the star formation rate (SFR) in galaxies evolves with redshift provides important constraints to the galaxy formation and evolution theories. In particular, semi-analytic models (SAMs; e.g. White & Frenk 1991; Kauffmann, White & Guiderdoni 1993; Springel et al. 2001; Monaco, Fontanot & Taffoni 2007; Guo et al. 2011; Benson et al. 2012; Menci, Fiore & Lamastra 2012; Henriques et al. 2013) need to be directly compared with observations to obtain insight of the relevant physical processes. The first and most popular SAMs are three, commonly named 'Munich' (starting with the models of Kauffmann et al. 1993), 'Durham' (beginning with the models of Cole et al. 1994), and 'Santa Cruz' (beginning with the models of Somerville & Primack 1999); more recent SAMs include, i.e. Croton et al. 2006; Bower et al. 2006; Somerville et al. 2008; Fontanot et al. 2009; Guo et al. 2011; Somerville et al. 2012. The main differences between these models lie in the prescriptions adopted for some of the most basic baryonic processes,

such as star formation, gas cooling, and feedback. One of the processes that must be modelled and compared to data is the evolution of the SFR over the cosmic time. However, the derivation of an accurate SFR from observational data is difficult, due to the many uncertainties involved in its reconstruction. An important source of uncertainty comes from dust extinction. The rest-frame ultraviolet (UV) light emitted by young and massive stars, strictly connected to the instantaneous SFR in galaxies, is strongly absorbed by dust, and re-radiated in the infrared (IR) bands. Dust attenuation, as well as other galaxy physical properties, evolve with cosmic time and show a peak between $z \sim 1$ and 2 (e.g. Burgarella et al. 2013). Knowing how dust attenuation evolves in redshift is therefore crucial to study the redshift evolution of the SFR: to this purpose, combining UV information with direct observations in the IR region is probably the best tool to account for the total SFR (e.g. Kennicutt 1998). In fact, IR surveys covering a wide range of redshifts are extremely useful to estimate the global IR luminosity, since they provide a direct measurement of the amount of energy absorbed and re-emitted by dust (e.g. what is missed by UV surveys).

Herschel (Pilbratt et al. 2010), with its 3.5 m mirror, has been the first telescope which allowed us to detect the far-IR

---

[*] E-mail: carlotta.gruppioni@oabo.inaf.it

population to high redshifts ($z \sim 3$–4) and to derive its rate of evolution through a detailed luminosity function (LF) analysis (Gruppioni et al. 2013; Magnelli et al. 2013) thanks to the extragalactic surveys provided by the Photodetector Array Camera and Spectrometer (PACS; Poglitsch et al. 2010) and Spectral and Photometric Imaging Receiver (SPIRE; Griffin et al. 2010) in the far-IR/sub-mm domain (i.e. PACS Evolutionary Probe, PEP, Lutz et al. 2011; *Herschel* Multi-tiered Extragalactic Survey, HerMES, Oliver et al. 2012; GOODS-*Herschel*, Elbaz et al. 2011; *Herschel*-ATLAS, Eales et al. 2010). PEP and HerMES are the major *Herschel* Guaranteed Time extragalactic key-projects, designed specifically to determine the cosmic evolution of dusty star formation and of the IR LF, and include the most popular and widely studied extragalactic fields with extensive multiwavelength coverage available (deep optical, near-IR, and *Spitzer* imaging, and spectroscopic and photometric redshifts; see Berta et al. 2011; Lutz et al. 2011; Oliver et al. 2012 for a detailed description of the fields and observations). The far-IR domain in galaxies, although potentially contaminated by the presence of an active galactic nucleus (AGN), has been probed to be dominated by star formation (i.e. Hatziminaoglou et al. 2010; Delvecchio et al. 2014). Therefore, PEP and HerMES, and all the ancillary data available in the fields, give us the opportunity to disentangle star formation from AGN contribution and to study in detail the evolution of the SFR with cosmic time since the Universe was about a billion years old.

In a recent paper from Pozzi et al. (2015), the observed IR PEP/HerMES LFs have been reproduced by means of a phenomenological model considering two galaxy populations characterized by different evolutions, i.e. a population of late-type sources and a population of protospheroids. In the model, the IR LFs (linked to the SFR) have been reproduced, as well as the literature *K*-band LFs (directly linked to the stellar mass), showing that most of the PEP-selected sources observed at $z > 2$ can be explained as progenitors of local spheroids caught during their formation.

Similar evolutionary rates have been found by Gruppioni et al. (2013), deriving the far- and total IR (i.e. rest frame 8–1000 μm) LFs from the *Herschel* data obtained within the PEP and HerMES projects up to $z \sim 4$. Since a large fraction of *Herschel*-selected objects have been found to contain an AGN (Berta et al. 2013; Gruppioni et al. 2013; Delvecchio et al. 2014), an accurate quantification of the AGN contribution to the IR luminosity is needed in order to derive reliable SFRs (e.g. not contaminated by AGN activity) from these sources. Delvecchio et al. (2014), through a detailed Spectra Energy Distribution (SED) decomposition analysis (see Berta et al. 2013), have disentangled the contribution to the total IR luminosity due to AGN activity and that due to SF for the whole PEP sample. By starting from the work of Delvecchio et al. (2014), but considering the contribution of SF only, in this paper we focus on the determination of the SFR function (SFRF) and SFR density (SFRD) and compare the results with the predictions of state-of-the-art SAMs of galaxy formation and evolution.

This paper is organized as follows. We discuss the PEP multiwavelength catalogue in Section 2 and the theoretical predictions and comparison with data in Section 3; finally we present our conclusions in Section 4.

Throughout this paper, we use a Chabrier (2003) initial mass function (IMF) and we assume a Λ-cold-dark-matter (ΛCDM) cosmology with $H_0 = 71$ km s^{-1} Mpc^{-1}, $\Omega_{\rm m} = 0.27$, and $\Omega_\Lambda = 0.73$ for data derivations. Note that, although not affecting the results of this paper (see e.g. Wang et al. 2008), the considered SAMs use slightly different cosmologies.

2 THE SFR FUNCTION OF *HERSCHEL*-SELECTED GALAXIES

2.1 The data set

We have considered the *Herschel* PACS (70, 100, and 160 μm) and SPIRE (250, 350, and 500 μm) data in the COSMOS and GOODS-S fields from the PEP and HerMES surveys and all the multiwavelength data set associated with the far-IR sources. The reference sample is the PEP blind catalogue selected at 160 μm to the 3σ level, which consists of 4118 and 492 sources, respectively, in COSMOS (to 10.2 mJy in $\sim$2 deg^2) and GOODS-S (to 1.2 mJy in $\sim$196 arcmin^2). As described in detail by Berta et al. (2011) and Gruppioni et al. (2013), our sources have been associated with the ancillary catalogues by means of a multiband likelihood ratio technique (e.g. Sutherland & Saunders 1992), starting from the longest available wavelength (160 μm, PACS) and progressively matching 100 μm (PACS), 70 μm (PACS, GOODS-S only), and 24 μm (*Spitzer*/MIPS). In the GOODS-S field, we have associated with our PEP sources the 24 μm catalogue by Magnelli et al. (2009, extracted with IRAC 3.6 μm positions as priors) that we have matched with the optical+near-IR+IRAC MUSIC catalogue of Grazian et al. (2006), revised by Santini et al. (2009), which includes spectroscopic and photometric redshifts. In COSMOS, we have matched our catalogue with the deep 24 μm sample of Le Floc'h et al. (2009) and with the IRAC-based catalogue of Ilbert et al. (2010), including optical and near-IR photometry and photometric redshifts. In HerMES a prior source extraction was performed using the method presented in Roseboom et al. (2010), based on MIPS 24 μm positions. The 24 μm sources used as priors for SPIRE source extraction are the same as those associated with our PEP sources through the likelihood ratio technique. We have therefore associated the HerMES sources with the PEP sources by means of the 24 μm sources matched to both samples. For most of our PEP sources ($\sim$87 per cent) we found a $>3\sigma$ SPIRE counterpart in the HerMES catalogues. Redshifts (either spectroscopic or photometric) are available for all the sources in GOODS-S and for 93 per cent of the COSMOS sample (references and details also in Berta et al. 2011 and Gruppioni et al. 2013).

2.2 The SFR function and SFR density

Gruppioni et al. (2013) derived the far- and total IR (i.e. rest frame 8–1000 μm) LFs from the *Herschel* data obtained within the PEP and HerMES projects up to $z \sim 4$. To compute the SFRF, we have used the same data and method used by Gruppioni et al. (2013) for deriving the total IR LF, but here we have subtracted – for each source individually – the AGN contribution from each SED, as estimated by Delvecchio et al. (2014), to obtain the IR luminosity due to SF only. In order to disentangle the possible AGN contribution from that related to the host galaxy, Delvecchio et al. (2014) have performed a broad-band SED decomposition of our PEP sources using the MAGPHYS code (da Cunha, Charlot & Elbaz 2008), which is a public code using physically motivated templates to reproduce the observed galaxy SEDs, as modified by Berta et al. (2013) to include also the AGN component (from Fritz, Franceschini & Hatziminaoglou 2006; Feltre et al. 2012 models). Delvecchio et al. (2014) found significant (at 99 per cent) contribution from AGN in 37 per cent of the PEP sources and used the IR luminosity of the AGN component to derive the AGN bolometric LF and the supermassive black hole (SMBH) growth rate across cosmic time up to $z \sim 3$. Note that Delvecchio et al. (2014) choose to derive the
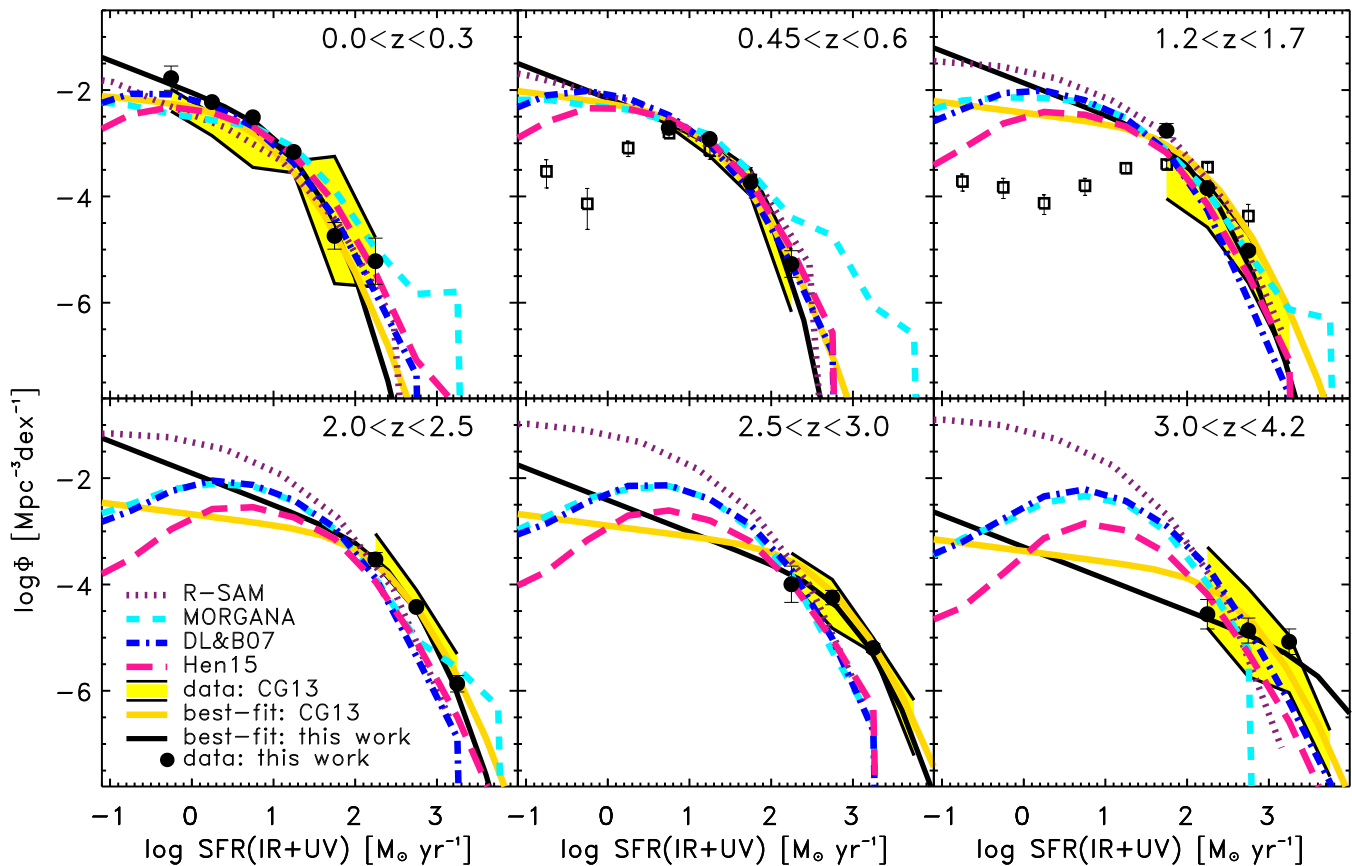
Figure 1. IR+UV SFRF estimated through the $1/V_{max}$ method in six representative redshift bins, by combining the data from the PEP GOODS-S and COSMOS fields using the Avni & Bahcall (1980) technique (black filled circles). The black solid line represents our best fit to our data with a modified Schechter function, while the yellow solid line is the total IR LF (without excluding AGN contribution through SED decomposition) obtained by Gruppioni et al. (2013), converted to an SFRF. The SFRFs of 24 μm sources with $\log(M/M_{\odot}) > 10$ in the GOODS-S by Fontanot et al. (2012) are plotted for comparison as black open squares. The SAMS predictions are shown as purple dotted (R-SAM), sea-green short-dashed (MORGANA), blue dot–dashed (De Lucia & Blaizot 2007) and deep-pink long-dashed (Henriques et al. 2015) coloured lines.

SMBH accretion function only up to $z \sim 3$, based on the fact that too few BH accretion data points were available at $z > 3$ in order to provide an acceptable fit. On the contrary, in this work, we subtract the AGN component from the total IR luminosity of the sources with a significant AGN activity to obtain the contribution due to SF only (L_{IR}^{SF}). In contrast with the work of Delvecchio et al. (2014), we can estimate the SFRF also in the $3 < z < 4.2$ interval, since the SFR data above the completeness limit allowed us to obtain an acceptable fit (though with larger uncertainties than at lower z). We have used the same calibration of Santini et al. (2009) and Papovich (2007) to estimate the total instantaneous SFR (then used to derive the SFRF):

$$\mathrm{SFR}_{IR+UV}/M_{\odot}\, \mathrm{yr}^{-1} = 1.8 \times 10^{-10} \times (2.2 \times L_{UV} + L_{IR}), \quad (1)$$

with $L_{UV} = 1.5 \times L_{2700\,\text{Å}}$ computed from the best-fitting template SED, and $L_{IR} = L_{IR}^{SF}$. To derive the SFRF, we have used the $1/V_{max}$ method (Schmidt 1968), combining the data in the two fields following Avni & Bahcall (1980). According to this method, the SFRF value and its uncertainty in each SFR bin have been computed as

$$\Phi(\mathrm{SFR}, z) = \frac{1}{\Delta \mathrm{SFR}} \left[\sum_i \frac{1}{w_i \times V_{max,i}} \pm \sqrt{\sum_i \frac{1}{(w_i \times V_{max,i})^2}} \right],$$
$$(2)$$

where $V_{max, i}$ is the comoving volume over which the ith galaxy could be observed, ΔSFR is the size of the SFR bin (in logarithmic scale), and w_i is the completeness correction factor of the ith galaxy. These completeness correction factors are a combination of the completeness corrections given by Berta et al. (2011), derived as described in Lutz et al. (2011), to be applied to each source as a function of its flux density, together with a correction for redshift incompleteness. Additional details are given in Gruppioni et al. (2013).

The resulting SFRFs in different redshift intervals are shown in Fig. 1 (black solid circles) and presented in Table 1 (together with their associated 1σ uncertainties). For comparison, the SFRF of sources with $\log(M/M_{\odot}) > 10$ in the GOODS-S derived by Fontanot et al. (2012) have been also plotted, although the two samples have different selections (i.e. the Fontanot et al. 2012 sample is selected at 24 μm and complete in mass, while ours is flux-limited at 160 μm), therefore are not directly comparable at the fainter SFRs (affected by the sample cuts). Our best-fitting solution with a modified Schechter function (Saunders et al. 1990) has also been reported (black solid line) and compared with the best fit to the total IR LF of Gruppioni et al. (2013, yellow solid line), converted to SFRF through the Kennicutt (1998) relation scaled to the Chabrier IMF (although containing also the AGN contribution).

Note that, apart from the two lower redshift bins ($z < 0.45$), the faint end of our SFRFs is not constrained by data; therefore,

Table 1. PEP SFRF and SFRD.

z	$\log(\Phi/\mathrm{Mpc}^{-3}\,\mathrm{dex}^{-1})$ $\log(\mathrm{SFR_{IR+UV}}/\mathrm{M_\odot\,yr^{-1}})$								$\mathrm{SFRD_{IR+UV}}$	$\mathrm{SFRD_{IR}}$ $(\mathrm{M_\odot\,yr^{-1}\,Mpc^{-3}})$
	−0.5–0.0	0.0–0.5	0.5–1.0	1.0–1.5	1.5–2.0	2.0–2.5	2.5–3.0	3.0–3.5		
0.0–0.3	−1.78 ± 0.23	−2.26 ± 0.05	−2.53 ± 0.04	−3.29 ± 0.05	−4.92 ± 0.31	−5.22 ± 0.43			0.025 ± 0.005	0.022 ± 0.016
0.3–0.45		−2.52 ± 0.14	−2.36 ± 0.11	−2.85 ± 0.08	−4.29 ± 0.11	−5.22 ± 0.31			0.035 ± 0.010	0.028 ± 0.012
0.45–0.6			−2.70 ± 0.09	−2.94 ± 0.06	−3.79 ± 0.05	−5.45 ± 0.31			0.049 ± 0.014	0.038 ± 0.013
0.6–0.8			−2.38 ± 0.19	−2.67 ± 0.06	−3.51 ± 0.03	−4.96 ± 0.13			0.056 ± 0.013	0.039 ± 0.015
0.8–1.0				−3.01 ± 0.08	−3.26 ± 0.04	−4.40 ± 0.06	−6.17 ± 0.43		0.064 ± 0.016	0.050 ± 0.019
1.0–1.2				−2.95 ± 0.11	−3.17 ± 0.08	−4.13 ± 0.04			0.062 ± 0.014	0.056 ± 0.026
1.2–1.7					−2.76 ± 0.13	−3.90 ± 0.04	−5.23 ± 0.08		0.082 ± 0.021	0.051 ± 0.025
1.7–2.0						−3.96 ± 0.10	−4.61 ± 0.05	−6.56 ± 0.43	0.071 ± 0.019	0.062 ± 0.023
2.0–2.5						−3.54 ± 0.13	−4.46 ± 0.06	−6.09 ± 0.19	0.062 ± 0.021	0.058 ± 0.015
2.5–3.0						−4.00 ± 0.34	−4.23 ± 0.13	−5.32 ± 0.10	0.056 ± 0.020	0.053 ± 0.016
3.0–4.2						−4.67 ± 0.28	−4.94 ± 0.20	−5.34 ± 0.32	0.028 ± 0.012	0.016 ± 0.012

we can only derive the value of α at low-z, then fix it and keep that value also in the higher redshift bins. This Hobson's choice implies the assumption that the faint-end slope does not vary with redshift. However, we note that at $z < 0.45$, where α is constrained by data, the SFRF obtained from the conversion of the total IR LF of Gruppioni et al. (2013) is flatter at low SFRs than the (IR+UV) SFRF (e.g. the yellow uncertainty area is lower than the faintest SFR data point). This can be interpreted as due either to a major contribution of the UV to the faint end (almost negligible at higher SFRs, dominated by the IR) or/and to the fact that some sources might move to fainter luminosity bins when the AGN contribution is removed, thus steepening the SFRF. The latter explanation is also consistent with our finding that in all the redshift bins but the highest one (which is also the most uncertain, due to the high fraction of photometric redshifts), the bright end of the SFRF (black solid line) is always steeper than that of the total IR LF converted to SFRF (yellow solid line). Since the AGN-dominated sources contribute mainly to the bright end of the IR LF (see Gruppioni et al. 2013), this difference is due to the subtraction of the AGN component from their SEDs.

The SFRF of 24-μm selected sources with $M > 10^{10}$ M$_\odot$ by Fontanot et al. (2012) is in good agreement with our determination, in the common redshift and SFR range, with the Fontanot et al. (2012) one being flatter in the lower SFR common bin, likely due to the mass cut in their sample.

By integrating the best-fitting modified Schechter function to our IR+UV (IR) SFRFs down to $\log_{10}(\mathrm{SFR}) = -1.5$ in the different redshift bins, from $z \sim 0$ to ~ 4, we have derived the comoving IR+UV (IR) SFRD, as presented in the tenth (last) column of Table 1 and shown in Fig. 2 as a grey filled (orange-line-filled) area. For comparison, other derivations from different bands are shown (i.e. the integration of the best-fitting Schechter function to the total IR LF, containing AGN, converted to SFR as yellow-line-filled area; the IR+UV SFRD by Burgarella et al. 2013 as dark-green filled area; the fit to optical/UV data by Behroozi et al. 2013 as pale-blue filled area; the UV SFRD – uncorrected for extinction – derivation by Cucciati et al. 2012 as blue-line-filled area).

From the comparison between our SFRD and previous derivations, we notice that the IR+UV SFRD estimated in this work is higher at low redshift (i.e. $z < 0.5$), while it agrees within the uncertainties with the other estimates at higher z. The IR-only SFRD, given the larger uncertainties, is consistent with the optical SFRD by Behroozi et al. (2013) and with the Gruppioni et al. (2013) IR luminosity density (LD) at low-z, although the average value is also

higher than the latter estimates. Therefore, the low redshift difference is likely due to the UV SFR contribution (that in percentage is higher at low-z), but mostly due to the AGN contribution subtraction. The (uncorrected for dust extinction) UV SFRD by Cucciati et al. (2012) is significantly lower than our IR or IR+UV one over the $0 < z < 3$ range, while at $z > 3$ it becomes comparable. This is consistent with the peak of dust extinction being around $z \sim 1.5$–2, with dust attenuation rapidly decreasing at higher redshifts (>3–4; e.g. Burgarella et al. 2013). In the *top panel* of Fig. 2 we also show the redshift evolution of the total SFRDs as obtained (from the same data sample) by Burgarella et al. (2013; dark-green shaded region). The differences (i.e. the Burgarella et al. 2013 estimate is lower than the current one at $z < 1$ and slightly higher, but still within the uncertainties, at $z > 2.5$) can be ascribed to the fact that in the previous analysis an average AGN contribution for each population had been subtracted from the total IR LD (then converted to SFRD and summed to the UV SFRD), while in this work an accurate object-by-object subtraction of the IR luminosity contribution due to the AGN has been performed, thanks to the detailed SED-fitting and decomposition of Delvecchio et al. (2014), and a proper SFRF has then been calculated from the obtained IR+UV SFRs.

Finally, we note that, while the best-fitting function to the co-moving SFRD from IR and UV data by Madau & Dickinson (2014) is in good agreement with our derivation (although slightly lower at $z < 0.5$ and higher at $z > 3$), at $z > 0.5$ the average Behroozi et al. (2013) estimate is always higher (although consistent within the large uncertainty region), maybe due to large extinction corrections.

Finally, in Fig. 2 we show the SFRD value obtained by Marchetti et al. (2015) from the HerMES wide-area sample, by combining the SFR from IR and UV (in analogy with this work), but without excluding the AGN contribution. The value is in good agreement with the result of Gruppioni et al. (2013, and the others from the literature) at the same redshift and only marginally consistent without IR+UV SFRD result.

3 SEMI-ANALYTICAL MODEL PREDICTIONS

In this section, we compare the observed SFRFs with results obtained with four SAMs of galaxy formation. The SAMs considered in this work are as follows: the MOdel for the Rise of Galaxies aNd Agns (MORGANA, Monaco et al. 2007; sea-green short-dashed lines in the figures), R-SAM (Menci et al. 2012; Menci, Fiore & Lamastra 2014; purple dotted lines), and two versions of the
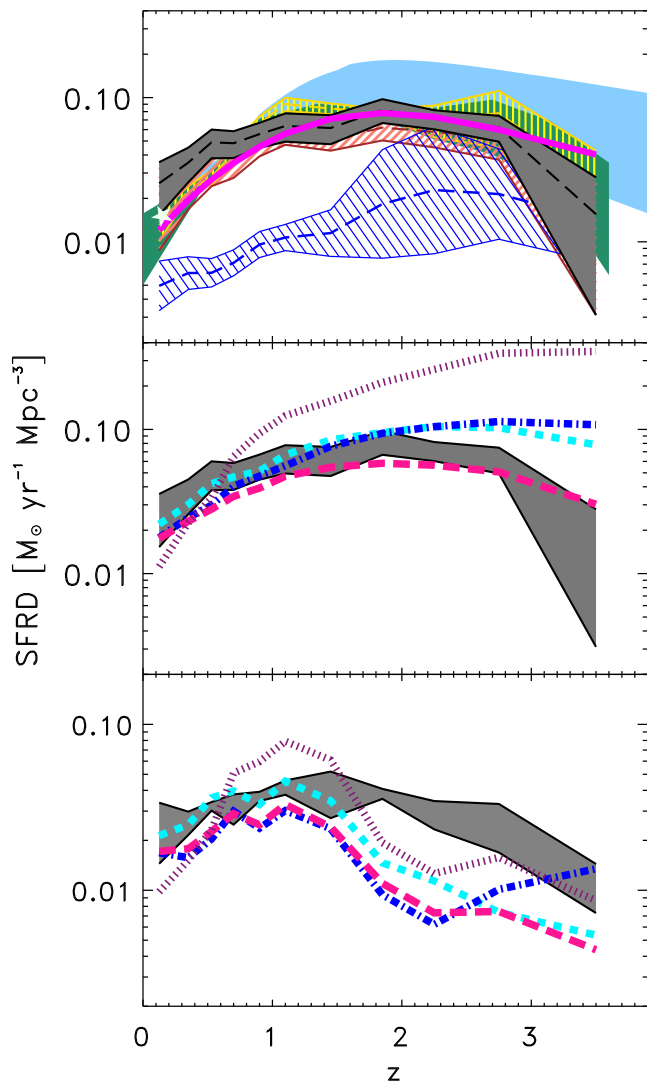
Figure 2. Redshift evolution of the comoving SFRD. The results of integrating the best-fitting curve for our observed IR+UV SFRD in each *z*-bin is shown as grey filled area (±1σ uncertainty locus). Top panel: our IR+UV SFRD estimate is compared with other derivations: the yellow-line-filled area shows the total IR luminosity density resulting from integrating the Gruppioni et al. (2013) best-fitting curve (i.e. converted to SFRD without excluding the AGN contribution); the orange-line-filled area shows the uncertainty region of the only IR SFRD from our data (after AGN removal); the blue-line-filled area is the uncorrected for extinction UV SFRD by Cucciati et al. (2012); the dark-green filled area is the Burgarella et al. (2013) estimate from *Herschel* data; the pale-blue filled area represents the fit to optical/UV data by Behroozi, Wechsler & Conroy (2013); the magenta line is the best-fitting function to IR and UV comoving SFRD by Madau & Dickinson (2014). The honeydew star shows the SFRD value obtained by Marchetti et al. (2015) from the HerMES local wide area sample, by combining the IR and the UV SFRs (but without excluding the AGN contribution). Middle panel: our IR+UV SFRD estimate shown in the previous panel is compared with the SAMs' predictions (same colours and line styles as in the previous figures) integrated over the same range of SFRs (from $\log_{10}(\mathrm{SFR}) = -1.5$). Bottom panel: same as in the previous panel, but with our best-fitting function and SAMs integrated only over the SFR range covered by our data.

Munich model[1] by De Lucia & Blaizot (2007; dot–dashed blue lines) and Henriques et al. (2015; deep-pink long-dashed lines). Note that these SAMs use slightly different cosmologies (see the relative papers for details), although this does not affect the results discussed in this paper (as shown by Wang et al. 2008). Moreover, all the SAMs' predictions (except the R-SAM ones) are mass-limited, with a cut at $M = 10^9$ M⊙, though this selection affects only the low SFRs, typically lower than those reached by our data. Since these models have not been 'tuned' to reproduce the SFRFs, the results shown in this work can be considered as genuine SAMs' predictions.

SAMs treat the physical processes involving baryons (thermal state and inflow/outflow of gas, star formation, feedback, accretion on to a BH, AGN feedback) within the backbone of dark matter (DM) halo merging histories, produced by the gravitational collapse of DM (see Benson 2010, for a review). We refer the reader to the papers cited above for all details on the models.

Together with the observational SFRF, Fig. 1 reports, at the six chosen redshift ranges, the SFRFs predicted by the four SAMs. To take into account the errors in the observational determination of SFRs, model predictions have been convolved with a fiducial error of 0.3 dex (assuming a lognormal error distribution for the SFR with an amplitude of 0.3 dex). As discussed by Fontanot et al. (2009, 2012), this value is roughly equal to the median formal error of SFRs in the GOODS-MUSIC catalogue (Santini et al. 2009) and allows us to determine the gross effect of (random) uncertainties in SFR determinations. We consider this value suitable also for our far-IR-based SFR.

At low redshift ($z < 1.7$, the three upper panels), all but MORGANA model predictions, are remarkably similar on the bright end. The MORGANA model at $z \lesssim 0.8$ shows an excess of very bright sources, that is connected to the specific model of radio-mode AGN feedback, where accretion on to the central BH takes place from the cold, star-forming gas in the bulge, so the suppression of star formation is partial. All models tend to give a power-law tail for the bright end of the SFRF, that is broadly compatible with the analytical extrapolation of the observed SFRF presented in Section 2. The broadly good agreement between models and data at the bright end breaks in the very important redshift range from 2 to 3, with the very steep SFRFs produced by all models becoming apparently different from the analytic fit to data in the highest redshift bin. However, the slope of this analytic fit is determined by $z = 0$–0.3 data, while at $z \gtrsim 2$, there is clear observational evidence of a steep (or even steepening of the) UV LF (e.g. Cucciati et al. 2012). The consistency at least of one of these models (e.g. MORGANA) with the LF of Lyman-break galaxies has been investigated by Lo Faro et al. (2009). At $z \gtrsim 2$, the models underpredict the bright end of the SFRF by a factor of ~0.2–0.3 dex. This result depends sensitively on the adopted modelling of observational error. Fig. 3 shows the comparison of models and data for two redshift bins at $z \sim 0$ and ~ 2, *without* convolving with 0.3 dex error. While the comparison at $z = 0$ remains acceptable, the disagreement at $z \sim 2$ worsens dramatically. Only extreme assumptions on the error on SFRs would allow us to recover the $z \simeq 2$ SFRF.

We stress that in the highest redshift bin ($3 < z < 4.2$), where the knee of the observed SFRF is not clearly detectable and the

---

[1] Obtained from the publicly available data base http://gavo.mpa-garching.mpg.de/Millennium/. The Millennium Simulation databases used in this paper and the web application providing online access to them were constructed as part of the activities of the German Astrophysical Virtual Observatory (GAVO; Lemson & the Virgo Consortium 2006).
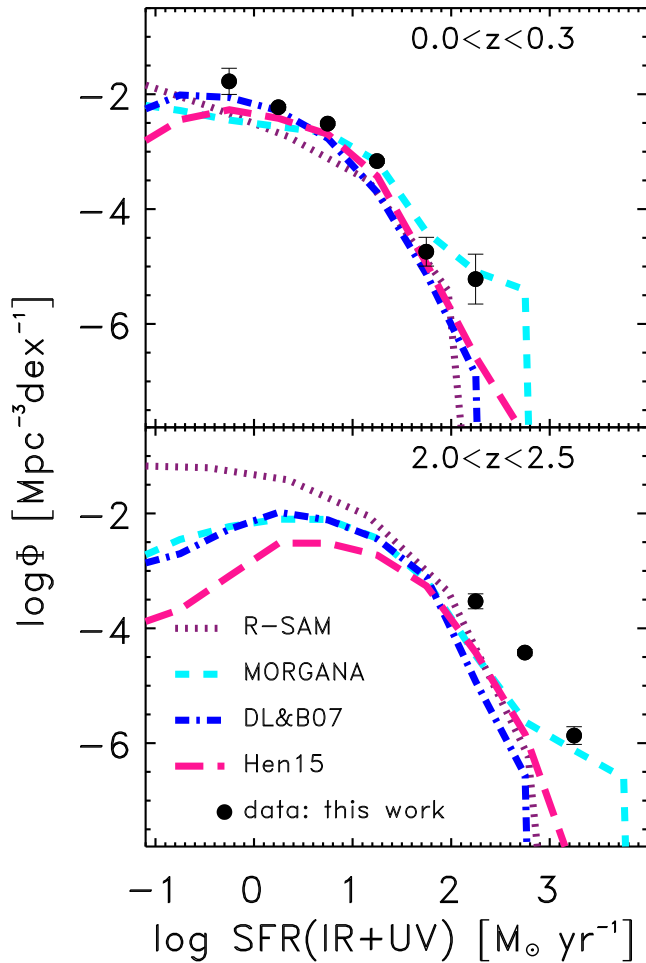
Figure 3. Total (IR+UV) SFRF (same as in Fig. 1; black filled circles) in two representative redshift bins compared to SAMs' predictions not convolved with an error of 0.3 dex (same colours and line styles as in Fig. 1).

shape seems to change significantly, the fraction of photometric redshifts and of the power-law SED AGN (with an uncertain photo-*z* determination) is higher than at lower *z*s. For this reason, this *z*-bin is more affected by uncertainties than the other ones and the discrepancy with model predictions here must be taken just as indications (to be further verified).

The inability of SAMs to reproduce the bright end of the *Herschel* LF at $z \gtrsim 2$ had previously been found by Niemi et al. (2012), though based on very preliminary *Herschel* LF results. It might be connected to the tendency of models to underestimate the main sequence of star-forming galaxies at $z \sim 2$ (e.g. Dutton, van den Bosch & Dekel 2010). Because SFRs are determined by the complex pattern of gas inflows and outflows, in and out DM haloes, and because inflows are determined by outflows taking place at previous times, identifying the cause of this disagreement is not easy. One possibility could be excessive feedback, possibly from AGN either in the radio mode (cooling and thus SFR is oversuppressed in these objects) or in the quasar mode (quasar-triggered outflows limit SFR); however, models with very different implementations of AGN feedback are showing the same problem. Alternatively, an excessive formation of stars in low-mass galaxies (Fontanot et al. 2009; Lo Faro et al. 2009; Weinmann, Neistein & Dekel 2011) could lock too much gas in stars instead of ejecting it from DM haloes and making it available for later star formation.

What is interesting to note is that, despite the very different prescriptions for SFR and stellar feedback, all models provide similar predictions (at least up to $z \sim 3$) in terms of number density of objects with moderate SFRs. Probably this reflects the fact that all the models are calibrated to reproduce the knee of the $z = 0$ galaxy luminosity/mass function.

At low SFRs ($\lesssim 1\, M_\odot\, yr^{-1}$), typically below the completeness limit of *Herschel* data, models start to separate, with R-SAM and Henriques et al. (2015) giving respectively the highest and lowest SFRFs. These differences may be due to a number of features: different modelling of stellar and AGN feedback, calibration procedure, treatment of merger trees (analytical or based on simulations). The turnover at low SFRs observed in all models but R-SAM is mostly due to incompleteness: models are complete in DM halo mass, that is tightly correlated with stellar mass, while the correlation with SFR is much broader and time-dependent, and this creates a very broad cut-off. While at $z = 0$ model SFRFs tend to be lower than the observed ones (as noticed, e.g. by Fontanot et al. 2009), at higher redshifts (but still below $z \sim 1.7$) they overshoot by a large factor the SFRF of Fontanot et al. (2012), derived for 24-μm selected sources with $M_\star > 10^{10}\, M_\odot$ in the GOODS-S (but are consistent, up to $z \sim 2$, with the analytic fit to our SFRF). Part of the difference with Fontanot et al. (2012) is due to the selection in stellar mass done in that paper, which produces a flattening (double-peaked) of the faint end, although the same paper shows that MORGANA cannot predict the drop in the SFRF at $\sim 1\, M_\odot\, yr^{-1}$.

The overprediction of models with respect to the analytic fit to data observed at $\log_{10}(SFR) \lesssim 1$–2, becoming more and more important with increasing redshift (although the faint-end slope of the observed SFRSs is fixed at the value found at $z \sim 0$), if confirmed by deeper data, could be due to the well-known excess of low/intermediate mass galaxies predicted by most SAMs with respect to observed mass functions (see i.e. Somerville & Primack 1999; Cole et al. 2000; Menci et al. 2002; Croton et al. 2006). This aspect is a result of the small-scale power excess typical of the ΛCDM power spectrum (e.g. Klypin et al. 1999; Moore et al. 1999; Menci et al. 2012; Calura, Menci & Gallazzi 2014). Some authors have suggested that a strong feedback from exploding supernovae can help limiting this excess, and alleviate the discrepancy between data and models at the smallest scales (e.g. Croton et al. 2006; Pontzen & Governato 2012).

The integrals of the SFRFs (SFRD, shown in Fig. 2, *middle* and *bottom* panels) confirm and better quantify the trends shown in Fig. 1. The SFRDs obtained by integrating the SAMs over the same luminosity range as our best-fitting SFRFs, are marginally low at $z = 0$ for three models out of four (the MORGANA prediction is very close to the observed one, but this is driven by the bright excess visible in Fig. 1). MORGANA and the two Munich models follow the evolution of the observed SFRD up to $z \simeq 2$, while the R-SAM prediction is significantly steeper, overpredicting the data estimate from $z \sim 0.6$ up to the higher redshifts. From $z = 2$ to 3 all models but Henriques et al. (2015) overpredict the observed SFRD (at 1σ uncertainty level) by a factor >2, with R-SAM diverging by a factor as high as 7–8. Note that if we consider a more conservative uncertainty level for our data (i.e. 3σ), the disagreement would be much less or even negligible.

Since the observed SFRD shown in the *upper* and *middle* panels of Fig. 2 is obtained by integrating the SFRFs down to SFR values not covered by data, we have also computed the SFRD (from both data and models) by performing the integration just in the SFR range where PEP data are available (as shown in the *bottom* panel). Here the trend of models underpredicting the observed SFRD at high *z* is

even more evident, with data values starting to be underestimated by SAMs at $z \sim 1.5$–1.8, but getting closer to model predictions (especially with the Henriques et al. 2015 and R-SAM ones) at $z \sim 3.5$ (although the better agreement of the $3.2 < z < 4$ SFRD might be due to the compensation of the underestimate of the bright end and the overestimate of the faint end of the SFRF).

We can conclude that our results at high-z confirm a tension between models and data that possibly points to a problem related to the common assumptions that are at the base of galaxy formation within the ΛCDM cosmogony. Given the good agreement between models and data at low-z, we can interpret these $z > 2$ tensions as a consequence of model assumptions (like, e.g. the SF law and efficiency, IMF shape) and parameters being calibrated with local observations, and then assumed invariant at higher redshift. It is indeed possible for some of these analytical approximations to have an intrinsic or acquired redshift dependence (through the evolution of the physical properties of model galaxies, see e.g. Fontanot 2014, where the predicted SFRFs for SAMs with variable IMFs are discussed). None the less, the fact that the largest discrepancies between data and models are seen for the $2 < z < 3$ interval, which represents a peak for both the cosmic SFR and the BH accretion, points to the treatment of SFR in extreme environments as a likely source of the tension. Indeed, the modelling of extreme environments, such as those associated with the strongest starburst is still highly uncertain, with many theoretical studies suggesting a different star formation regime for these systems (see e.g. Somerville, Primack & Faber 2001; Hopkins et al. 2010).

On the other hand, also possible source of uncertainty in the data (affecting mainly the highest redshift interval) might contribute to the tension, increasing the bright end of the observed SFRF: they can be due to wrong photometric redshifts, bright IR sources at confusion level with flux enhanced by 'blending', misidentification of lensed galaxies (the latter only to a very minor extent, since the 160 μm selection should be much less affected by lensed galaxies than sub-mm wavelength ones; e.g. Negrello et al. 2007).

In future, deeper far-IR observations will be fundamental to explore the faintest end of the SFRF, whereas a study of the bright end at larger redshifts will provide tighter constraints on the feedback processes regulating star formation in the brightest galaxies. A combined study of SFRF and mass function will be also crucial in order to fully understand and tune the single processes considered in SAMs.

4 CONCLUSIONS

Starting from the far-IR PEP data considered by Gruppioni et al. (2013), in this paper we investigate the evolution of the SFRF in the redshift range $0.1 < z < 4$ and compare it with theoretical results from various SAMs of galaxy formation (MORGANA, R-SAM, De Lucia & Blaizot 2007, and Henriques et al. 2015). To compute the SFRF, we have subtracted the AGN contribution estimated by Delvecchio et al. (2014) from each SED, to obtain the IR luminosity due to SF only. Then, we have obtained the total instantaneous SFR by combining the IR SF luminosity with the UV derived one, to obtain the total (IR+UV) SFR, which we have considered to derive the SFRF.

The conclusions of our work can be summarized as follows.

(i) We find a generally good agreement between the observed and predicted SFRFs up to $z \sim 2$ (once the observational errors are taken into account in SAMs), with the exception of MORGANA, showing a high-SFR excess at $z \lesssim 0.8$. This result implies that theoretical models, despite the different prescriptions, are able to reproduce the space-density evolution of the IR luminous galaxies from the SFRD peak epoch up to now.

(ii) At $z \gtrsim 2$, all the models start to underpredict the bright end of the SFRF. This can be due to improper modelling of several ingredients that determine the inflow/outflow patterns of gas in/from DM haloes, like AGN feedback, limiting SFR in the largest galaxies, or even inefficient feedback from a previous generation of galaxies.

(iii) Our data are able to constrain the low-SFR end of the (IR+UV) SFRF only at low-z ($z < 0.45$). In this range of redshift, the observed slope is consistent with model predictions, but is steeper than the slope of the total IR LF (containing also AGN contribution) by Gruppioni et al. (2013). However, at intermediate/high-z, *Herschel* data do not sample the low-SFR end of the SFRF, where SAM predictions differ most: our data are not deep enough to allow us to distinguish between the different approaches to SF and stellar feedback considered by the different models. Additional sources of uncertainty affecting the models could be due to the fact that no evolution with redshift is considered for local relations and functions, as SFR laws and IMF. Finally, also data at high redshift could be affected by wrong photometric redshifts and source confusion, contributing to enhance the bright end of the SFRF, therefore the discrepancy with model predictions.

In this work we have shown that SFRF may help putting stringent constraints on the physical processes modelled in SAMs, especially if extended to low SFRs, while a study of the bright end at larger redshifts will provide tighter constraints on the feedback processes regulating star formation in the brightest galaxies. A combined study of SFRF and mass function will be crucial in order to fully understand and tune the single processes modelled in SAMs and to have a global picture of the evolution of SFR and mass growth in galaxies.

REFERENCES

Avni Y., Bahcall J. N., 1980, ApJ, 235, 694
Behroozi P. S., Wechsler R. H., Conroy C., 2013, ApJ, 770, 57
Benson A. J., 2010, Physics Reports, 495, 33
Benson A. J., Borgani S., De Lucia G., Boylan-Kolchin M., Monaco P., 2012, MNRAS, 419, 3590
Berta S. et al., 2011, A&A, 532, 49
Berta S. et al., 2013, A&A, 551, 100
Bower R. G., Benson A. J., Malbon R., Helly J. C., Frenk C. S., Baugh C. M., Cole S., Lacey C. G., 2006, MNRAS, 370, 645
Burgarella D. et al., 2013, A&A, 554, 70
Calura F., Menci N., Gallazzi A., 2014, MNRAS, 440, 2066
Chabrier G., 2003, ApJ, 586, L133
Cole S., Aragon-Salamanca A., Frenk C. S., Navarro J. F., Zepf S. E., 1994, MNRAS, 271, 781
Cole S., Lacey C. G., Baugh C. M., Frenk C. S., 2000, MNRAS, 319, 168
Croton D. J. et al., 2006, MNRAS, 365, 11
Cucciati O. et al., 2012, A&A, 539, A31

da Cunha E., Charlot S., Elbaz D., 2008, MNRAS, 388, 1595

De Lucia G., Blaizot J., 2007, MNRAS, 375, 2

Delvecchio I. et al., 2014, MNRAS, 439, 2736

Dutton A. A., van den Bosch F. C., Dekel A., 2010, MNRAS, 405, 1690

Eales S. et al., 2010, PASP, 122, 499

Elbaz D. et al., 2011, A&A, 533, 119

Feltre A., Hatziminaoglou H., Fritz J., Franceschini A., 2012, MNRAS, 426, 120

Fontanot F., 2014, MNRAS, 442, 3138

Fontanot F., De Lucia G., Monaco P., Somerville R. S., Santini P., 2009, MNRAS, 397, 1776

Fontanot F., Cristiani S., Santini P., Fontana A., Grazian A., Somerville R. S., 2012, MNRAS, 421, 241

Fritz J., Franceschini A., Hatziminaoglou E., 2006, MNRAS, 366, 767

Grazian A. et al., 2006, A&A, 449, 951

Griffin M. et al., 2010, A&A, 518, L3

Gruppioni C. et al., 2013, MNRAS, 423, 23

Guo Q. et al., 2011, MNRAS, 413, 101

Hatziminaoglou E. et al., 2010, A&A, 518, L33

Henriques B. M. B., White S. D. M., Thomas P. A., Angulo R. E., Guo Q., Lemson G., Springel V., 2013, MNRAS, 431, 3373

Henriques B. M. B., White S. D. M., Thomas P. A., Angulo R. E., Guo Q., Lemson G., Springel V., Overzier R., 2015, MNRAS, preprint (arXiv:1410.0365)

Hopkins P. F., Younger J. D., Hayward C. C., Narayanan D., Hernquist L., 2010, MNRAS, 402, 1693

Ilbert O. et al., 2010, ApJ, 709, 644

Kauffmann G., White S. D. M., Guiderdoni B., 1993, MNRAS, 264, 201

Kennicutt R. C., Jr, 1998, ApJ, 498, 541

Klypin A., Gottlöber S., Kravtsov A. V., Khokhlov A. M., 1999, ApJ, 516, 530

Le Floc'h E. et al., 2009, ApJ, 703, 222

Lemson G., the Virgo Consortium, 2006, preprint (arXiv:astro-ph/0608019)

Lo Faro B., Monaco P., Vanzella E., Fontanot F., Silva L., Cristiani S., 2009, MNRAS, 399, 827

Lutz D. et al., 2011, A&A, 532, 90

Madau P., Dickinson M., 2014, ARA&A, 52, 415

Magnelli B., Elbaz D., Chary R. R., Dickinson M., Le Borgne D., Frayer D. T., Willmer C. N. A., 2009, A&A, 496, 57

Magnelli B. et al., 2013, A&A, 553, A132

Marchetti L. et al., 2015, MNRAS, submitted

Menci N., Cavaliere A., Fontana A., Giallongo E., Poli F., 2002, ApJ, 575, 18

Menci N., Fiore F., Lamastra A., 2012, MNRAS, 421, 2384

Menci N., Fiore F., Lamastra A., 2014, A&A, 569, 37

Monaco P., Fontanot F., Taffoni G., 2007, MNRAS, 375, 1189

Moore B., Ghigna S., Governato F., Lake G., Quinn T., Stadel J., Tozzi P., 1999, ApJ, 524, L19

Negrello M., Perrotta F., Gonzlez-Nuevo Gonzalez J., Silva L., De Zotti G., Granato G. L., Baccigalupi C., Danese L., 2007, MNRAS, 377, 1557

Niemi S.-M., Somerville R. S., Ferguson H. C., Huang K.-H., Lotz J., Koekemoer A. M., 2012, MNRAS, 421, 1539

Oliver S. et al., 2012, MNRAS, 424, 1614

Papovich C. et al., 2007, ApJ, 668, 45

Pilbratt G. et al., 2010, A&A, 518, L1

Poglitsch A. et al., 2010, A&A, 518, L2

Pontzen A., Governato F., 2012, MNRAS, 421, 3464

Pozzi F. et al., 2015, ApJ, 803, 35

Roseboom I. G. et al., 2010, MNRAS, 409, 48

Santini P. et al., 2009, A&A, 504, 751

Saunders W., Rowan-Robinson M., Lawrence A., Efstathiou G., Kaiser N., Ellis R. S., Frenk C. S., 1990, MNRAS, 242, 318

Schmidt M., 1968, ApJ, 151, 393

Somerville R. S., Primack J. R., 1999, MNRAS, 310, 1087

Somerville R. S., Primack J. R., Faber S. M., 2001, MNRAS, 320, 504

Somerville R. S., Hopkins P. F., Cox T. J., Robertson B. E., Hernquist L., 2008, MNRAS, 391, 481

Somerville R. S., Gilmore R. C., Primack J. R., Domínguez A., 2012, MNRAS, 423, 1992

Springel V., White S. D. M., Tormen G., Kauffmann G., 2001, MNRAS, 328, 726

Sutherland W., Saunders W., 1992, MNRAS, 259, 413

Wang J., De Lucia G., Kitzbichler M. G., White S. D. M., 2008, MNRAS, 384, 1301

Weinmann S. M., Neistein E., Dekel A., 2011, MNRAS, 417, 2737

White S. D. M., Frenk C. S., 1991, ApJ, 379, 52

This paper has been typeset from a TEX/LATEX file prepared by the author.